



HAL
open science

Anisotropic bimodal distribution of blocking temperature with multiferroic BiFeO₃ epitaxial thin films

C. K. Safeer, M. Chamfrault, J. Allibe, C. Carretero, C. Deranlot, E. Jacquet, J.-F. Jacquot, M. Bibes, A. Barthelemy, B. Dieny, et al.

► **To cite this version:**

C. K. Safeer, M. Chamfrault, J. Allibe, C. Carretero, C. Deranlot, et al.. Anisotropic bimodal distribution of blocking temperature with multiferroic BiFeO₃ epitaxial thin films. *Applied Physics Letters*, 2012, 100, pp.072402. 10.1063/1.3684812 . hal-01683669

HAL Id: hal-01683669

<https://hal.science/hal-01683669>

Submitted on 23 May 2019

HAL is a multi-disciplinary open access archive for the deposit and dissemination of scientific research documents, whether they are published or not. The documents may come from teaching and research institutions in France or abroad, or from public or private research centers.

L'archive ouverte pluridisciplinaire **HAL**, est destinée au dépôt et à la diffusion de documents scientifiques de niveau recherche, publiés ou non, émanant des établissements d'enseignement et de recherche français ou étrangers, des laboratoires publics ou privés.

Anisotropic bimodal distribution of blocking temperature with multiferroic BiFeO₃ epitaxial thin films

C. K. Safeer,¹ M. Chamfrault,¹ J. Allibe,² C. Carretero,² C. Deranlot,² E. Jacquet,² J.-F. Jacquot,³ M. Bibes,² A. Barthélémy,² B. Dieny,¹ H. Béa,^{1,a)} and V. Baltz^{1,b)}

¹SPINTEC, Unité Mixte de Recherche CEA/CNRS/UJF associée à Grenoble INP, INAC 17 rue des Martyrs, 38054 Grenoble Cedex, France

²Unité Mixte de Physique CNRS/Thales, 1 Avenue Fresnel, Campus de l'Ecole Polytechnique, 91767 Palaiseau, France and Université Paris-Sud, 91405 Orsay, France

³INAC SCIB, F-38054 Grenoble 9, France

(Received 29 November 2011; accepted 25 January 2012; published online 13 February 2012)

Controlling BiFeO₃ (BFO)/ferromagnet (FM) interfacial coupling appears crucial for electrical control of spintronic devices using this multiferroic. Here, we analyse the magnetic behaviour of exchange-biased epitaxial-BiFeO₃/FM bilayers with in-plane or out-of-plane magnetic anisotropies. We report bimodal distributions of blocking temperatures similar to those of polycrystalline-antiferromagnet (AF)/FM bilayers. The high-temperature contribution depends on the FM anisotropy direction and is likely related to thermally activated depinning of *domain walls* in the BiFeO₃ single crystal film as opposed to thermally activated reversal of spins in AF *grains* for polycrystalline AF. In contrast, the low-temperature contribution weakly depends on the anisotropy direction, consistent with a spin-glass origin. © 2012 American Institute of Physics. [doi:10.1063/1.3684812]

Controlling a magnetic state by an electric field could give rise to magnetoelectric random access memories (MERAMs),¹ which would be a breakthrough for spintronics applications. Such an electrical control of magnetism^{2,3} (e.g., *via* the magnetoelectric effect⁴) may offer significant advantages over today's approaches for controlling magnetization switching i.e., by magnetic field or spin transfer torque. One of the few room temperature (T) single phase multiferroic^{5,6} candidates is BiFeO₃ (BFO), a material that displays magnetoelectric coupling⁷⁻⁹ and is both antiferromagnetic (AF) and ferroelectric.

Because BFO is AF, it has to be exchange coupled to an adjacent ferromagnet (FM) layer¹⁰⁻¹² to be implemented in magnetoelectric memory prototype. Practically, the AF order of BFO can be modified by applying an electric field via the magnetoelectric coupling and this change in AF can then act on the FM magnetisation direction.^{13,14} A magnetic exchange bias (EB) between BFO and a FM has been observed at room T for FM layers with in-plane magnetic anisotropy such as NiFe,¹⁰ CoFeB,¹¹ and CoFe.¹² In contrast, out-of-plane exchange bias coupling has not been observed so far. It is important to further investigate this point since this magnetic orientation would offer better down size scalability than in-plane anisotropy in spintronic devices.¹⁵ This EB coupling typically results in a shift of the hysteresis loop of the FM along the magnetic field axis used to set the exchange bias direction.¹⁶ This shift strongly depends on T and disappears for T above the so-called blocking temperature (T_B). In the case of polycrystalline AF/FM heterostructures, it was shown that the T_B distribution (DT_B) presents a bimodal character,¹⁷ with a high-T contribution attributed to

grains¹⁸ and a low-T contribution ascribed to interfacial spin-glass phases.¹⁹

In this letter, we first discuss EB results for BFO/CoFeB thin films, for which BFO is epitaxially grown on SrTiO₃ substrates. A fundamental difference between polycrystalline AF and epitaxial BFO films is that the spin lattice in BFO has a homogeneous exchange stiffness with the possible formation of AF domains whereas polycrystalline AF such as IrMn exhibits an uncoupled grain behaviour wherein each grain can be considered as single domain with no interaction with the neighbouring grains. Despite this major difference, we observed bimodal DT_B in BFO/CoFeB bilayers similar to those previously observed in polycrystalline AF/FM bilayers. Second, we compare DT_B for samples with FM layers with in-plane or out-of-plane magnetic anisotropy. We evidence that the DT_B is anisotropic, which yields us (1) to conclude that BFO uncompensated interfacial spins lie in the sample plane and (2) to support the interfacial spin-glass origin of the low-T contribution.

BFO thin films of various thicknesses (15, 70, and 250 nm) were epitaxially grown on SrTiO₃ (001) substrates by pulsed laser deposition, as described in Ref. 20. FM layers were subsequently sputter-deposited *ex situ*. A saturating in-plane magnetic field H_{dep} was applied along the [100] direction during anisotropy FM deposition: CoFeB (4 nm) and Co (3 nm). Out-of-plane field was used for out-of-plane anisotropy FM: [Co (0.4 nm)/Pt (1.8 nm)]_{x4}. Au (6 nm) and Pt (2 nm) capping layers were additionally sputtered on top of CoFeB (4 nm) and Co (3 nm), respectively, in order to avoid oxidation. Magnetic hysteresis loops along the anisotropy direction were measured by superconducting quantum interference device (SQUID) magnetometry either at 300 K in the as deposited state or at 2 K following specific thermal field cooling (FC) procedures in order to deduce DT_B as described below. Care has been taken in order to measure

^{a)}Electronic mail: helene.bea@cea.fr.

^{b)}Electronic mail: vincent.baltz@cea.fr.

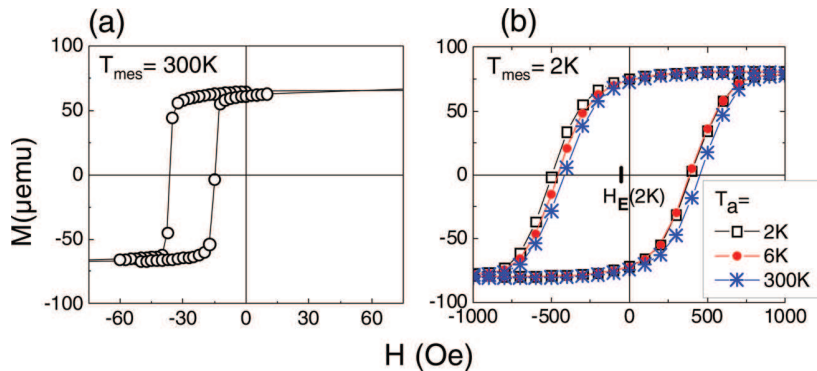


FIG. 1. (Color online) In-plane hysteresis loops for BFO (15 nm)/CoFeB (4 nm) sample (a) measured at $T_{\text{mes}} = 300$ K and (b) at $T_{\text{mes}} = 2$ K after the specific field cooling procedure from several T_a .

and correct the data from a reproducible remanent magnetic field of 2 Oe due to trapped vortex in the superconducting coils of the SQUID. We have also checked that the samples display no systematic training effect (i.e., when repeating several times a hysteresis loop, we observe no systematic decrease of loop shift).

Fig. 1(a) shows a typical hysteresis loop measured in-plane, along the deposition field at a measuring temperature (T_{mes}) of 300 K, for a film of BFO (15 nm)/CoFeB (4 nm). In agreement with previous studies,^{10–12} a finite H_E is observed at room T. This primarily indicates that the maximum T_B of the system is above 300 K. We then determined DT_B between 2 and 375 K following the procedure initially suggested in Ref. 21. Note that the data are reproducible in this T range (above 375 K, the sample starts to be magnetically irreversibly modified). First, we perform a FC from 300 K down to $T_{\text{mes}} = 2$ K with a positive magnetic field of +1 T parallel to H_{dep} . This is done so as to orient positively all the BFO pinned uncompensated spins $S_{\text{AF},p}$ (see arrows sketched in Fig. 2(a)). An hysteresis loop is then measured at 2 K. One reaches the maximum obtainable amplitude for H_E at 2 K, H_E being negative, $-H_{E,\text{max}}$. This corresponds to the loop of Fig. 1(b) for 2 K. From this initial magnetic state, the procedure then consists in applying a temperature T_a (between 4 and 375 K) followed by a FC down to 2 K under a negative magnetic field (-1 T) antiparallel to H_{dep} for incremental T_a . Note that T_a is often called annealing temperature in the literature. For each T_a , the BFO uncompensated spins whose T_B are smaller than T_a are reoriented towards the negative direction (see arrows sketched in Fig. 2(a)). After each increment of T_a , an hysteresis loop is measured at 2 K. H_E is proportional to the difference between the amount of BFO pinned uncompensated spins initially oriented towards the positive direction and those reoriented towards the negative direction. When T_a increases, a gradual

change in the amplitude and sign of H_E is observed since more and more BFO pinned uncompensated spins have been reoriented. This is what one sees in Fig. 1(b) that shows typical hysteresis loops measured at 2 K after various T_a . If the same amount of pinned uncompensated spins are oriented positively and negatively, $H_E = 0$. Note that if T_a is larger than the maximum T_B of the system, one expects to recover a maximum amplitude of H_E but with opposite sign as compared to the initial state: $+H_{E,\text{max}}$ (see arrows sketched in the negative direction in Fig. 2(a)). From Fig. 1(b), note also that H_C is around 430 Oe and remains independent on T_a , within a 5% window. This is consistent since T_{mes} remains the same for every hysteresis loop.¹⁷

The gradual change of H_E is better visible in the dependence of H_E on T_a plotted in Fig. 2(a) for BFO (t_{BFO})/CoFeB (4 nm) samples with BFO thicknesses, t_{BFO} of 15 and 70 nm. We repeated the procedure several times for some T_a . The small discrepancy in the values gives an error bar for H_E [see for example the two data points at $T_a = 300$ K in Fig. 2(a)]. For both samples, the amplitude of H_E does not reach $H_{E,\text{max}}$ for $T_a = 375$ K. This means that DT_B extends above 375 K. Unfortunately, we cannot reach this part of the distribution due to sample damaging beyond this T. This is possibly due to layers intermixing and it notably results in a reduction of H_C at $T_{\text{mes}} = 2$ K accompanied by irreproducible data. From Fig. 2(a), two inflections are clearly visible for both t_{BFO} , one at low-T (below 100 K) and one at high-T (above 300 K). This reflects two contributions to DT_B [see Fig. 2(b)], which results from the derivative of $H_E/H_{E,\text{max}}$ with respect to T_a .¹⁷ When several data points were measured for the same T_a , we used the average value in order to calculate DT_B . DT_B for epitaxial BFO/CoFeB is quite similar in shape to those of fully polycrystalline samples.¹⁷ In the latter case, the high-T contribution to DT_B is ascribed to the thermally activated reversal of decoupled or weakly coupled AF grains.

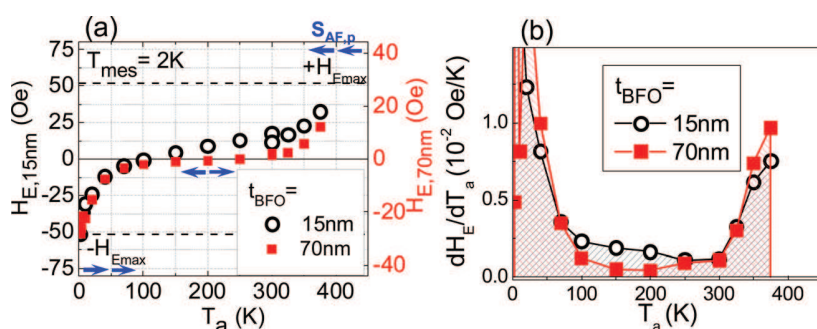


FIG. 2. (Color online) (a) Dependence of H_E on T_a for BFO (t_{BFO})/CoFeB (4 nm) with $t_{\text{BFO}} = 15$ and 70 nm. The dashed horizontal lines represent the extremum values for H_E . The arrows represent the orientation of BFO pinned uncompensated spins at different T_a . (b) Dependence on T_a of the derivative of normalized H_E : $\delta H_E / \delta T_a$. $\delta H_E / \delta T_a$ vs T_a represents the blocking temperature distribution.

The distribution in the grain volumes is proportional to the high-T contribution to DT_B . In the present case, the AF is a single crystal for which AF domains are separated by domain walls instead of grain boundaries. The high-T contribution thus has a different origin here. It is likely ascribed to the thermally activated depinning of domain walls within the AF BFO layer. We can notice in Fig. 2(b) that the high-T contribution does not seem to significantly shift towards larger T when the AF thickness is increased as this contribution starts around the same T. For thinner fully polycrystalline AF/FM (Ref. 17) increasing the AF thickness results in enhancing the volume of decoupled or weakly coupled AF grains. This shifts the distribution of grain volumes towards larger values, which accounts for the concomitant observation of a shift of DT_B towards higher T. We point out that even for polycrystals, the shift of the high-T contribution to DT_B does not linearly depend on the AF thickness but rather levels off for thick AF.²² Note that for the BFO (250 nm)/Co (3 nm) sample that we discuss below, the high-T contribution to DT_B shown in Fig. 3(c) is also consistent with the above observations, namely the high-T contribution to DT_B for thick epitaxial BFO/FM bilayers is weakly affected by t_{BFO} .

In order to further investigate the AF entities at the origin of the two distinct contributions in DT_B , we compared measurements between BFO/FM with FM layers having distinct anisotropy directions. We used Co based FM with either in-plane anisotropy: Co (3 nm) or out-of-plane anisotropy: [Co (0.4 nm)/Pt (1.8 nm)]_{×4}.²³ In [001] oriented BFO films, if the cycloidal modulation is altered,^{24–26} the spins are theoretically expected to lie within the (111) planes, i.e., perpendicular to the electrical polarization. They would thus present both in-plane and out-of-plane components. If such a spin structure is preserved from the bulk of BFO up to its surface, non-zero exchange coupling should be observable for BFO/FM, irrespective of the FM anisotropy direction. Surprisingly, at room T, only the system with in-plane

anisotropy shows non-zero H_E [insets of Figs. 3(a) and 3(b)]. In order to better understand this anisotropic behaviour of BFO/FM bilayers, we have deduced DT_B [see Fig. 3(c)] from H_E vs T_a measurements [shown in Figs. 3(a) and 3(b)] for both samples and following the procedure detailed above. In both cases, a low-T contribution is present (corresponding to the large change of $H_E(T_a)$ below 100 K) similar to the cases of Fig. 2. However, one observes a striking difference between the two samples above 200 K. In Fig. 3(a), for the out-of-plane case, H_E reaches $+H_{E\max}$ around 150-200 K and displays no change above. It indicates that 150-200 K is around the maximum T_B . This is consistent with the zero H_E measured at 300 K. Note again that repeated measurements give an idea of the error bars. In Fig. 3(c), the above observations translate as follows: within error bars, for FM with out-of-plane anisotropy, BFO/FM does not display any high-T contribution to DT_B . We point out that due to sample damaging as discussed above, the T_a range for BFO/[Co/Pt]_{×4} is limited to 2 to 350 K. In the in-plane case, between 150 and 300 K, H_E follows a plateau, but has not reached $+H_{E\max}$. Another increase in H_E occurs above 300 K. It approaches $+H_{E\max}$ for $T_a = 375$ K. This is consistent with the non zero H_E at 300 K and it translates into a high-T contribution to DT_B [see Fig. 3(c)]. We note that this is similar to the situation in the 15 and 70 nm BFO samples despite the use of different FM layers with in-plane anisotropy: Co and CoFeB. From the anisotropic DT_B shown in Fig. 3(c), we can thus stress the following two points. (1) The high-T contribution is associated with AF entities that do not couple with spins oriented out-of-plane. This could be explained by an in-plane direction of BFO spins contributing to EB. BFO spins at the interface, thus point in the (001) plane perpendicular to the growth direction and not in the (111) expected plane for the underlying bulk BFO. Either they reorient between the bulk of the film and the surface or they lie in the (001) plane in the whole film due to the strain imposed by the substrate. (2) The low-T contribution is associated with AF entities that can more easily orient towards in- and out-of-plane directions. This is consistent with a spin-glass origin with lower anisotropies as already evoked for polycrystals.^{17,19} We note here that the peculiar spin structure as evidenced above, namely an in-plane reorientation of BFO uncompensated spins might also contribute to the formation of frustrated regions at the BFO/FM interface, in addition to the other believed origins of frustrations like roughness or structural defects for example. While it is relevant to discuss the relative amplitude of the high- and low-T contribution to DT_B for a given sample, we note that it might be hazardous here to compare the absolute amplitude for the two samples shown in Fig. 3. If the nominal AF/FM interface is BFO-Co for both samples, the real interface is certainly more complex. For the sample with out-of-plane anisotropy, notably, the interface is definitely closer to a BFO-CoPt_x in reality.²⁷

To conclude, we evidenced that EB in epitaxial-BFO/FM bilayers display bimodal DT_B alike fully polycrystalline AF/FM. As the low-T contribution remains unaffected by the FM anisotropy, its origin would be consistent with spin-glass regions. These spin-glass entities do not contribute to H_E at the device operating T. An objective is now to decrease their amount as much as possible to maximize H_E at the operating

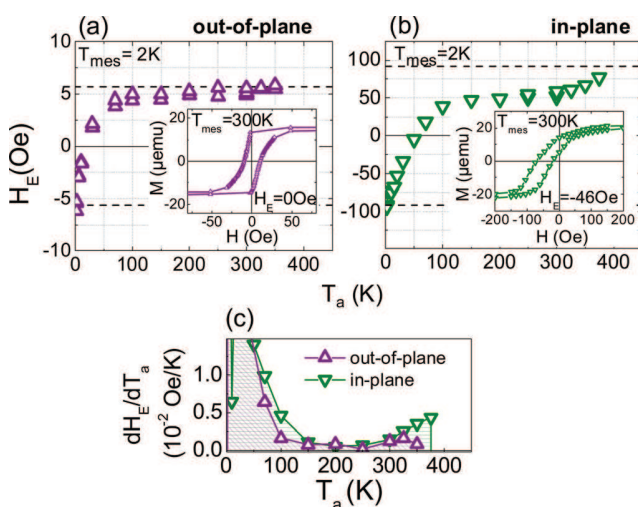


FIG. 3. (Color online) Dependence of H_E on T_a measured along the anisotropy axis for (a) BFO (250 nm)/[Co (0.4 nm)/Pt (1.8 nm)]_{×4} with out-of-plane anisotropy and for (b) BFO (250 nm)/Co (3 nm) with in-plane anisotropy. The insets are hysteresis loops measured at $T_{mes} = 300$ K along the deposition field axis. (c) Dependences on T_a of the derivatives of normalized H_E : $\delta H_E / \delta T_a$.

T.^{28,29} In contrast to polycrystalline AF/FM, the high-T contribution is certainly driven here by thermally activated depinning of domain walls in the AF layer as opposed to thermally activated magnetic reversal of spins in decoupled AF grains for polycrystals. Despite these fundamental origins, we observed that the high-T contribution behaves quite similarly. Finally, we have shown that this high-T contribution depends on the FM magnetic anisotropy, suggesting an in-plane orientation of interfacial BFO spins. This prevents out-of-plane EB with epitaxial BFO deposited on (001) SrTiO₃, which explains the absence of much literature on this point despite the advantages of the use of out-of-plane anisotropy in allowing a better down size scalability of spintronic devices over systems with in-plane anisotropy.¹⁵ Efforts have yet started in order to circumvent this drawback and to force out-of-plane anisotropy of interfacial BFO spins.

The authors thank J. Ben Youssef and T. Hauguel from the laboratoire de magnétisme de Bretagne at Brest for fruitful discussions. H.B. acknowledges the CNRS for the chaire CNRS grant.

¹M. Bibes and A. Barthélémy, *Nature Mater.* **7**, 425 (2008).

²Y. Shiota, T. Nozaki, F. Bonell, S. Murakami, T. Shinjo, and Y. Suzuki, *Nature Mater.* **11**, 39 (2011).

³W. G. Wang, M. Li, S. Hageman, and C. L. Chien, *Nature Mater.* **11**, 64 (2011).

⁴M. Fiebig, *J. Phys. D* **38**, R123 (2005).

⁵W. Eerenstein, M. D. Mathur, and J. F. Scott, *Nature* **442**, 759 (2006).

⁶N. A. Spaldin and M. Fiebig, *Science* **309**, 391 (2005).

⁷G. Catalan and J. F. Scott, *Adv. Mater.* **21**, 2463 (2009).

⁸D. Lebeugle, D. Colson, A. Forget, M. Viret, A. M. Bataille, and A. Gukasov, *Phys. Rev. Lett.* **100**, 227602 (2008).

⁹T. Zhao, A. Scholl, F. Zavaliche, K. Lee, M. Barry, A. Doran, M. P. Cruz, Y. H. Chu, C. Ederer, N. A. Spaldin *et al.*, *Nature Mater.* **5**, 823 (2006).

¹⁰J. Dho, X. Qi, H. Kim, J. L. MacManus-Driscoll, and M. G. Blamire, *Adv. Mater.* **18**, 1445 (2006).

¹¹H. Béa, M. Bibes, S. Cherifi, F. Nolting, B. Warot-Fonrose, S. Fusil, G. Herranz, C. Deranlot, E. Jacquet, K. Bouzehouane *et al.*, *Appl. Phys. Lett.* **89**, 242114 (2006).

¹²L. W. Martin, Y. H. Chu, Q. Zhan, R. Ramesh, S. J. Han, S. X. Wang, M. Warusawithana, and D. G. Schlom, *Appl. Phys. Lett.* **91**, 172513 (2007).

¹³Y. H. Chu, L. W. Martin, M. B. Holcomb, M. Gajek, S. J. Han, Q. He, N. Balke, C. H. Yang, D. Lee, W. Hu *et al.*, *Nature Mater.* **7**, 478 (2008).

¹⁴J. T. Heron, M. Trassin, K. Ashraf, M. Gajek, Q. He, S. Y. Yang, D. E. Nikonov, Y. H. Chu, S. Salahuddin, and R. Ramesh, *Phys. Rev. Lett.* **107**, 217202 (2011).

¹⁵S. Mangin, D. Ravelosona, J. A. Katine, M. J. Carey, B. D. Terris, and E. E. Fullerton, *Nature Mater.* **5**, 210 (2006).

¹⁶J. Nogués and I. K. Schuller, *J. Magn. Magn. Mater.* **192**, 203 (1999).

¹⁷V. Baltz, B. Rodmacq, A. Zarefy, L. Lechevallier, and B. Dieny, *Phys. Rev. B* **81**, 052404 (2010).

¹⁸E. Fulcomer and S. H. Charap, *J. Appl. Phys.* **43**, 4190 (1972).

¹⁹K. Takano, R. H. Kodama, A. E. Berkowitz, W. Cao, and G. Thomas, *Phys. Rev. Lett.* **79**, 1130 (1997).

²⁰H. Béa, M. Gajek, M. Bibes, and A. Barthélémy, *J. Phys. Condens Matter.* **20**, 434221 (2008).

²¹S. Soeya, T. Imagawa, S. Mitsuoka, and S. Narishige, *J. Appl. Phys.* **76**, 5356 (1994).

²²V. Baltz, J. Sort, S. Landis, B. Rodmacq, and B. Dieny, *Phys. Rev. Lett.* **94**, 117201 (2005).

²³M. T. Johnson, P. J. H. Bloemen, F. J. A. den Broeder, and J. J. de Vries, *Rep. Prog. Phys.* **59**, 1409 (1996).

²⁴C. Ederer and N. A. Spaldin, *Phys. Rev. B* **71**, 060401R (2005).

²⁵F. Bai, J. Wang, M. Wuttig, J. Li, N. Wang, A. P. Pyatakov, A. K. Zvezdin, L. E. Cross, and D. Viehland, *Appl. Phys. Lett.* **86**, 032511 (2005).

²⁶H. Béa, M. Bibes, S. Petit, J. Kreisel, and A. Barthélémy, *Philos. Mag. Lett.* **87**, 165 (2007).

²⁷L. Lechevallier, A. Zarefy, R. Lardé, H. Chiron, J.-M. Le Breton, V. Baltz, B. Rodmacq, and B. Dieny, *Phys. Rev. B* **79**, 174434 (2009).

²⁸V. Baltz and B. Dieny, *J. Appl. Phys.* **109**, 066102 (2011).

²⁹V. Baltz, S. Auffret, and B. Dieny, *IEEE. Trans. Magn.* **47**, 3308 (2011).